Numerical study of the effect of winglet on the aerodynamic performance of sinusoidal and simple leading edge wings

M.Naderinezhad and M.H. Djavareshkian

Department of Mechanical Engineering, Ferdowsi University of Mashhad, Mashhad, Iran

Corresponding author:
MH Djavareshkian, Ferdowsi University of Mashhad, Faculty of Engineering, Vakilabad Ave., Mashhad 9177948974, Iran.
Email: javareshkian@um.ac.ir

Abstract:

Purpose –In this study, the effectiveness of two types of winglets, Multi-tip and Raked on the performance of sinusoidal and simple leading edge wings has been investigated and compared by a numerical method.

Design/methodology/approach – The wing configuration in this study is rectangular and uses NACA0020 section and all simulations are performed by a numerical method based on finite volume and base pressure algorithm in Reynolds $\mathbf{2 \times 10^5}$. In the mentioned numerical method, the flow is considered turbulent and the $\boldsymbol{k-\omega-SST}$ model is used. To calculate the stresses on the wing surface, the mesh is extended to below the viscous layer, and a second-order upstream accuracy is used to calculate the convection flux.

Findings –The use of Raked and Multi-tip winglets for the sinusoidal edge of the wing improved aerodynamic performance by 5.12 and 2.28 percent, respectively, and the greatest effect of these two winglets was on increasing the lifting force and reducing the inductive drag, respectively. Also, by examining the distribution of induced vortices around the configurations, it was found that the curvature of the sinusoidal wing tip at the angles of attack before stall reduced the strength of the induced vortices and, the use of winglet during and after stall, caused increased aerodynamic performance of the sinusoidal wing.

Practical implications – The whale is an international species of aquatic animal found in most of the world's oceans. It has large fin aspect ratios that have a series of bulges at the edge of the attack,

which improves aerodynamic performance near and after stall. Today, one of the fields of research is the use of this idea in the wings of MAWs.

Originality/value –Winglet reduces induced drag in simple wings. So far, the effect of winglets on wings with sinusoidal attack edges has not been investigated.

Keywords: Winglet, Induced drag, Aerodynamic performance, Sinusoidal edge attack wing, Vortex.

1. Introduction

The winglet is now well known as a useful mechanism for increasing the aerodynamic performance of the wing and reducing the fuel consumption of commercial aircraft, and various configurations have been designed and built from it (Chambers, 1990; Merryisha and Rajendran, 2019; Whitcomb, 1976; Gongzhang and Axtelius, 2020; Guerrero *et al.*, 2020). The installation of a blended winglet with a curved edge, which is a special type of Whitcomb winglet, has increased $C_{L\max}$ in the Reynolds of the transition range, and the difference between the aerodynamic coefficients has increased with increasing Reynolds number and the mounting angle of the bulk relative to the horizontal direction of the wing opening (Hossain *et al.*, 2011). According to the research on birds of prey, the ratio of wingspan without winglet and with multi-tip winglet (b_{cw} / b_w) should be in the range of 4 to 8 (Savile, 1957). For this reason, by inspiring the size of the wings of a bird of prey, a new type of multi-tip winglet was designed. The results of this study show that the designed winglet has the lowest induced delay generation in all tested attack angles. It also increases the slope of the diagram $C_{L-\alpha}$ by 7.25% for a distance of 20% of the chord length from the main wing between the winglet blades (Lynch, 2017).

Variables such as cant angle, tip span, the distance between the tip, and their arrangement have the greatest impact on the aerodynamic performance of multi-tip winglets. According to various studies on the performance of this type of winglet, the installation of the blades from the edge of attack to escape and their angle to the horizon is better from small to large has had the most aerodynamic performance (Bravo-Mosquera *et al.*, 2018; Sharafi, 2015; Narayan and Bibin, 2016; Zhang *et al.*, 2020). Due to the high performance of the corrugated wing to control the flow, several studies have been performed to show the effect of the wave leading edge on the wing as an inactive flow control system. This research showed that aerodynamic performance is increased in the stall area (Carreira Pedro and Kobayashi, 2008; New and Ng, 2020; Mehraban *et al.* 2021; Yasuda, 2019). The aerodynamic performance of a whale's wing in both smooth and sinusoidal attack edge modes at Reynolds numbers 505000 and 520000 for 2- to 20 ° attack angles in a subsonic wind tunnel has been investigated by Miklosovich *et al.* (2004). Preventing a sharp decrease in lifting force, increasing pressure drag force during the stall and a 40% increase in stall angle for the sinusoidal edge of the wing are among the results of this study.

According to the results of the study of Johari *et al.* (2007) the wing with a sinusoidal edge reduces the lift and increases the drag at attack angles less than stall. But at post-stall angles, it will increase the lifting force by 50% with the least increase in drag force. Thus, the sinusoidal wing increases the lift to drag ratio in the post-stall range. Also, to study the effect of amplitude size and wavelength on the performance of the attacking edge with sine waves, the amplitude of 25 to 50%

and the wavelength of 2 to 12.5% of the chord wing length were evaluated. The results show that the amplitude is more effective than the wavelength, more flow adhesion at the peaks at stall angles, and reduced slope of the darg diagram to the angle of attack due to increased wave amplitude (Zverkov *et al.*, 2008; Horton, 1968). To study more precisely the reason for the performance of wavy wings than simple wings in the stall areas, Zverkov *et al.*, 2008 have studied the differences between the boundary layer characteristics presented in Figure 1 around simple and wavy wings. The existence of a fundamental difference in the transition zone between the two configurations and the different behavior of flow physics at different peaks are among the findings of this study.

In research done so far, the effect of the winglet on the sinusoidal leading-edge wings has not been investigated. This study aims to investigate the effect of two winglets on the wing with a sinusoidal leading-edge in Reynolds 2.0×10^5. Also, the effect of these winglets on the aerodynamic performance of two simple and sinusoidal leading-edge wings is compared. In order to further match the selected Reynolds numbers and the geometric characteristics of the winglet with the real conditions of the bird for the present study, the flight characteristics of the red-tailed hawk with two winglet (multi-tip and raked) have been used (Table 1). In the results section, by extracting the aerodynamic coefficients and describing the flow physics, the effect of two winglets on the performance of the sinusoidal attack edge wing in comparison with the simple wing is investigated.

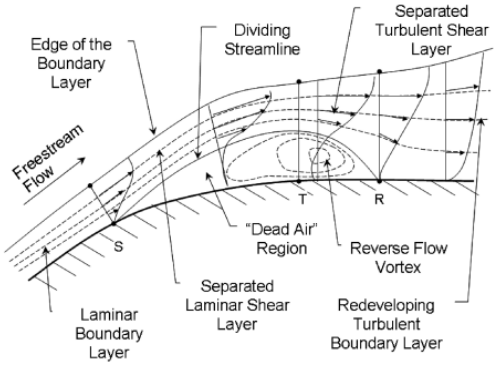

Figure 1: Laminar Separated bubble character (Horton, 1968)

Table 1: Geometric characteristics and flight range of birds of prey (Dunning, 2007**)**

Name and Characteristics Birds	Gyrfalcon	Falcon	Red-Tailed Hawk	Eagle
Span(cm)	110-130	74-120	105-141	180-234
Chord(cm)	34.5-41	26.5-39	32.5-44.5	52-72
AR	3.2-3.1	2.79-3	3.23-3.1	3.4-3.25
Reynolds range(10^5)	5.15-6.2	3.24-4.81	1.98-2.74	4.42-6.17

2. Numerical simulation Method

In the present simulation, the Reynolds-Averaged Navier-Stokes (RANS) equations are discretized using the finite volume method and then are solved. For coupling the velocity and pressure terms,

the SIMPLE algorithm was used (Versteeg and Malalasekera, 2007). Diffusion flux terms with the central difference method and convection flux terms with second-order upstream have been discretized. In all simulations, the unsteady and incompressible form of the equations is used. The $k\omega - SST$ model has been used to calculate Reynolds stress in all simulations of the present study. The reason for using this model is to extract results close to experimental data in research around simple wings and the sinusoidal leading edge with the help of this model (Narayan and Bibin, 2016; Roy and Mukherjee, 2020; Aftab *et al.* 2016). The main structure of this model consists of two equations for calculating the perturbation energy and the dissipation rate using the function F_1 for the correct guess of the flow according to the flow physics as follows (Wilcox, 1988).

$$\frac{\partial \rho k}{\partial t} + \frac{\partial}{\partial x_i}\left(\rho u_i k\right) = \frac{\partial}{\partial x_i}\left\{\left(\mu + \frac{\mu_{turb}}{\sigma_k}\right)\frac{\partial k}{\partial x_i}\right\} + \tau_{ij}^{R}\frac{\partial u_i}{\partial x_j} - \beta^{*}\rho\omega k \quad (١)$$

$$\frac{\partial \rho \omega}{\partial t} + \frac{\partial}{\partial x_i}\left(\rho u_i \omega\right) = \frac{\partial}{\partial x_i}\left\{\left(\mu + \frac{\mu_{turb}}{\sigma_k}\right)\frac{\partial \omega}{\partial x_i}\right\} + \frac{\gamma}{\mu_{turb}}\tau_{ij}\frac{\partial u_i}{\partial x_i} - \rho\beta\omega^2 + 2\rho\left(1-F_1\right)\sigma_{\omega_2}\frac{1}{\omega}\frac{\partial k}{\partial x_j}\frac{\partial \omega}{\partial x_j} \quad (٢)$$

Equations (3) are used to calculate the aerodynamic coefficient. In this relation, the value of these coefficients is calculated from the velocity and density (ρ_∞, V_∞) of free flow and the reference surface of the wing (S_{ref}).

$$C_L = \frac{L}{0.5\rho_\infty {V_\infty}^2 S_{ref}}$$
$$C_D = \frac{D}{0.5\rho_\infty {V_\infty}^2 S_{ref}} \quad (٣)$$

The power distribution of the induced vortices on the back wing plates is calculated using equation (4). According to this equation, the power of vortices based on their angular velocity (ω) per unit 1/s is considered. Due to the turbulence of the fluid flow, the shear stress is calculated according to Equation (5) on the configuration surface (Munson *et al.* 2016). Equation (6) is used to calculate the percentage of relative numerical and experimental error.

$$|\omega| = \sqrt{\omega_x^2 + \omega_y^2 + \omega_z^2} \quad (٤)$$

$$\tau = \tau_{lam} + \tau_{turb} = \mu_\infty \frac{\partial u}{\partial y}_{y=0} - \overline{\rho u' v'} \quad (٥)$$

$$\%Error = \frac{\left(C_{L_{EXP}} - C_{L_{NUM}}\right)}{C_{L_{EXP}}} * 100 \quad (٦)$$

3. Geometry and Solution Domain

In the present work, a rectangular wing with a cross-section of NACA 0020 and an aspect ratio of 2 is numerically simulated in Reynolds 2×10^5 and validated with experimental data. After

validating the numerical structure, two types of configuration of Multi-tip and Raked winglet with a length of 75 mm in the direction of the wingspan were added and evaluated to investigate their effects on the simple and sinusoidal leading-edge wings. The geometric profile of the sine wave edge is selected by considering the better aerodynamic performance of the sinusoidal wing in the stall range. The ratio of wavelength and amplitude to chord wing length is 0.5 and 0.06, respectively, and the sine wave equation used is shown in Figure 2 (Munson *et al*. 2016). In this equation, A and λ represent the amplitude and wavelength, which are calculated about different values of the wingspan length along the axis, and the value of the chord length was considered constant and equal to 144 mm.

$$x = c + A\sin[2\pi(\frac{z}{\lambda} - \frac{\lambda}{2c})]$$

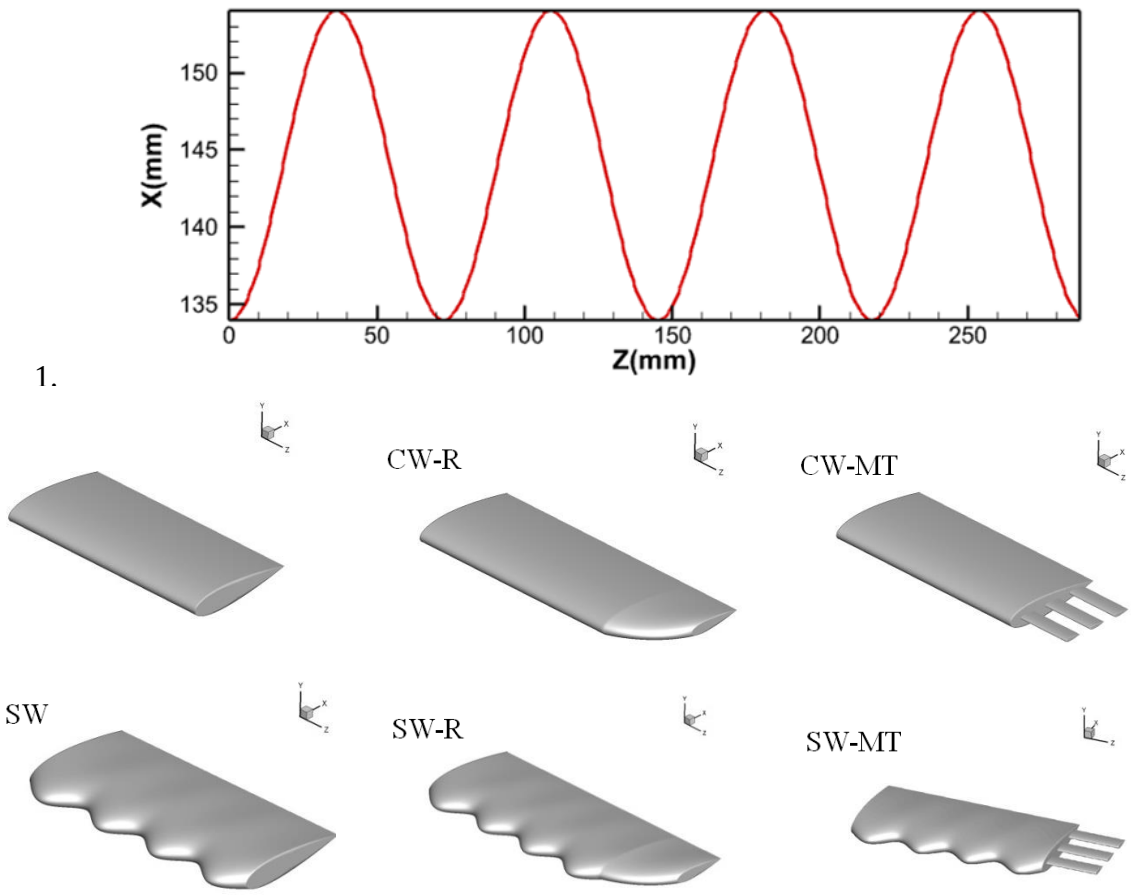

Figure 2: Equation and wave leading edge and configurations examined in the present study

The solution Domain is of C-H type and its boundaries have been developed as 12.5 and 20 times the chord length of the wing (Hassan *et al.*, 2014). Due to the simulation of incompressible flow in the present work, the input speed limit condition has been used. To simulate the effects of three-dimensional flow, such as induced vortices and spanwise flow, the side wall is spaced from the wingtip. Other specifications of the simulated boundary conditions and flow are presented in Figure 3.

To completely cover the waves of the leading edge and prevent the reduction of cell quality, the structure mesh is used as Figure 4-a, and to achieve the allowable range of Y Plus for the used turbulence model, the distance from the first cell to the surface of the wing is approximately equal to 0.01 mm (Figure 4-b).

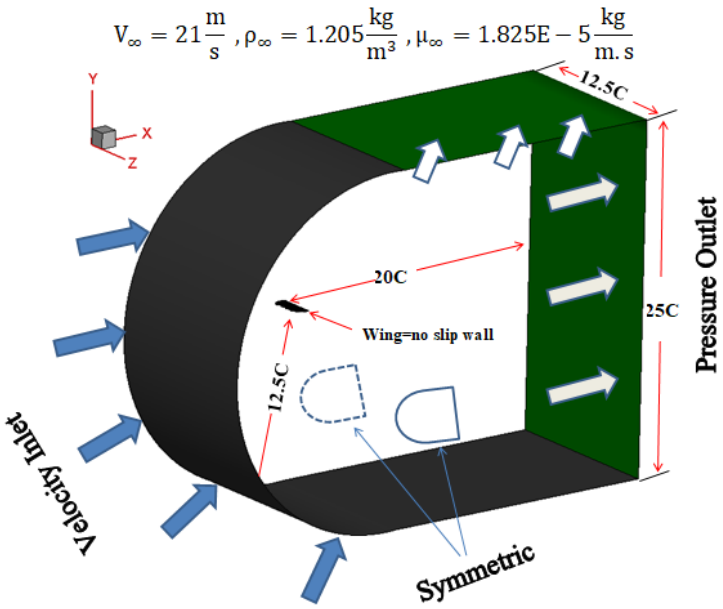

Figure 3: Numerical Domain and Boundary condition

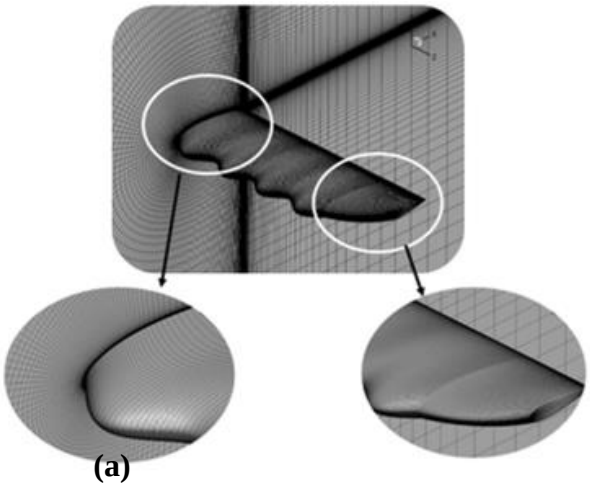

(a)

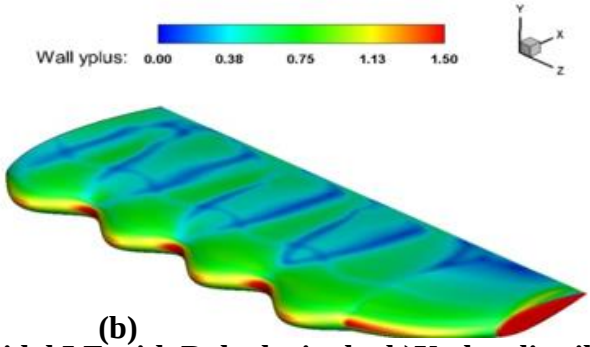

(b)

Figure 4: a) Mesh around Sinusoidal LE with Raked winglet b)Y plus distribution around the wing

In the present study, to reduce the computational error and achieve a suitable mesh, the process of mesh independence has been performed at angles close to the simple wing stall (attack angle of 16 degrees). This is due to the presence of reducing the accuracy of numerical models in the correct approximation of the starting point of separation of the boundary layer (due to shear stresses and unsteady drag force) at angles of the stall and flow physics around the sinusoidal wing, to increase the reliability of different mesh produced for other configurations.

The mentioned process was performed during the increase of mesh density around a simple wing with a ratio of 1.6 (on average) and the results are presented in Figure 5. The process of reducing the computational error due to the increase in mesh quality is quite evident in this image. Due to the small difference between 6.4 and 10 million mesh in calculating the coefficient of comparison with the computational volume, mesh by 6.4 million elements is used. The error in Figure 5 is calculated using Equation (6) and from comparison with reference experimental data (Abrantes, 2017).

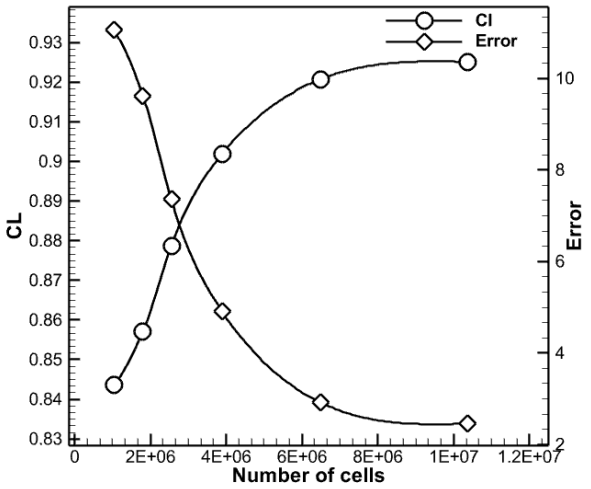

Figure 5: Independence lift coefficient of the mesh

To select the appropriate time step from the points of view of optimal simulation time and appropriate convergence range, different time steps are examined and their results are compared with each other in table 2. In this simulation, time step 1.25×١٠^{-٣} is selected.

Table 2: Results from the simulation of a rectangular wing at different time steps

Time Step	Cd	CL
2.5×١٠^{-٣}	0.0315	٠,٣٥٤
1.25×١٠^{-٣}	0.0294	٠,٣٥٢٥
6.52×١٠^{-٤}	0.0295	٠,٣٥٠٦
3.12×١٠^{-٤}	0.٠312	0.3511
1.56×١٠^{-٤}	0.0324	0.3487

To validate, the results of the simulation are compared with the experimental data related to the study of the reference rectangular wing (Hassan *et al*., 2014) with a turbulence intensity of 0.15% in Figure 6. Due to the importance of correct physics of the problem, in addition to quantitative validation, in Figure 6, the flow lines obtained from the numerical solution at 18 degrees are compared with the flow detection (by tuft). The results of this simulation show the similarity of the location of the central vortex core, the starting of separation from the root, and the effect of inductive vortices on the wingtip flow lines with experimental results (Figure 6)

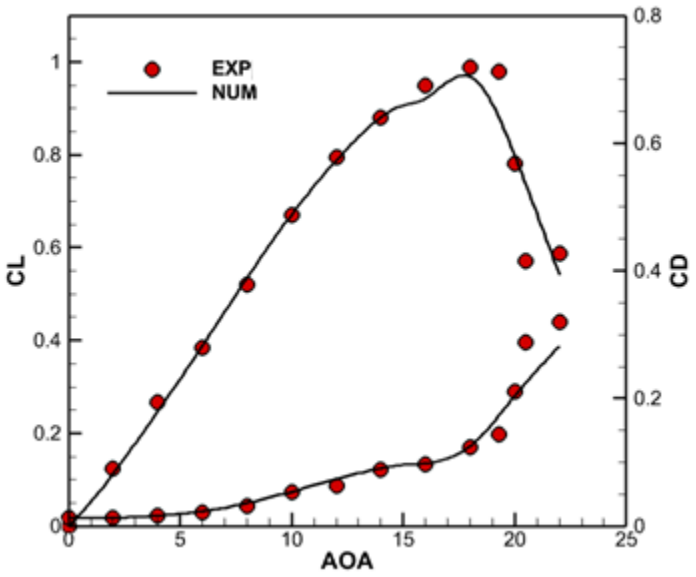

Figure 6: Comparison of numerical methods and experimental data (Abrantes ,٢٠١٧)

Visualization Over Rectangular wing

By Tuft

By Smoke

EXP

NUM

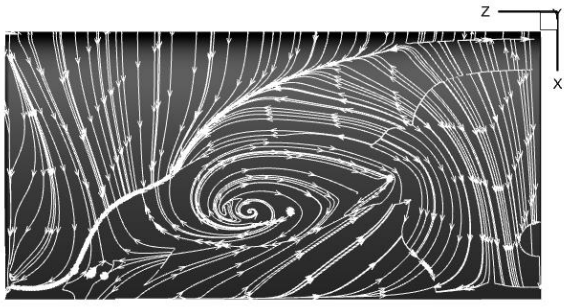

Figure 7: Streamline validation for in AOA=18 deg

4. Discussion and Results

In this section, the flow and behavior of induced vortices in the areas of collision with the winglet and the upper surface of the simple and sinusoidal wings are investigated. Also, the distribution of

pressure, qualitative and quantitative aerodynamic performance in stall range, and evaluation of the behavior of streamline after incidence with the winglet for specific distances from the trailing edge are presented. The configurations of this section are named based on the figure 2.

4.1. Lift Coefficient

According to Figure 8, the use of a Multi-tip winglet for simple wings has reduced the lifting force at all angles of attack. Based on the pressure distribution shown in Figure 9, each of the Multi-tip blades is affected by the other blade, and due to the interference of the flow with the two starting blades and the scattering of the flow lines, the pressure difference around the end blade decreases and reduces the lifting force. On the other hand, the presence of a Multi-tip winglet in this type of wing increases the wingspan and increases the $Cl - \alpha$ slope and changes the flow arrangement, which leads to a two-degree reduction (table 3) for the stall angle(16^o). But in the wing with the edge of the sinusoidal attack, there have been different changes. Because the deformation of the flow lines on the wing surface of the sinusoidal edge increases the pressure on the surface, the coefficient of lift force applied to this wing is reduced relative to the simple wing. Another effect of the deformation of flow lines is the formation of vortices with the direction of reverse motion on the surface of the sinusoidal wing after the flow collides with the attacking edge, which is considered as the main feature of this type of wing. This feature reduces the lift force on a simple sinusoidal wing and reduces the stall intensity at a 20-degree angle for wingless wings. However, as can be seen in Figure 8 (b), using a Multi-tip winglet to the sinusoidal wing, the stall angle has been increased by several degrees, while the stall angle in the simple wing with a Multi-tip winglet has been reduced by several degrees. As can be seen in Figure 8-a, the use of a Raked winglet for a simple wing before stall has increased the lifting force, and in the case of a sinusoidal wing with a Raked winglet, an increase in lift force can be seen in all angles of attack. At pre-stall angles, both wing and winglet configurations are affected by a greater pressure difference than by the non-winglet, and the maximum difference occurs at an angle of 18 degrees. After stalling for simple wings with and without winglets due to the rapid growth of separation, the lifting force is accompanied by a sharp decrease, but in the sinusoidal wing, the slope of the lifting force was less. At an angle of 20 degrees, due to the onset of the stall when using a Raked winglet for a simple wing, a larger part of the wing with winglet is affected by separation, and as a result, a lower amount of lifting force is produced than the wing without winglet. Quantitatively, the use of a Raked winglet in a sinusoidal wing can increase the lift coefficient by 19% in the stall angle.

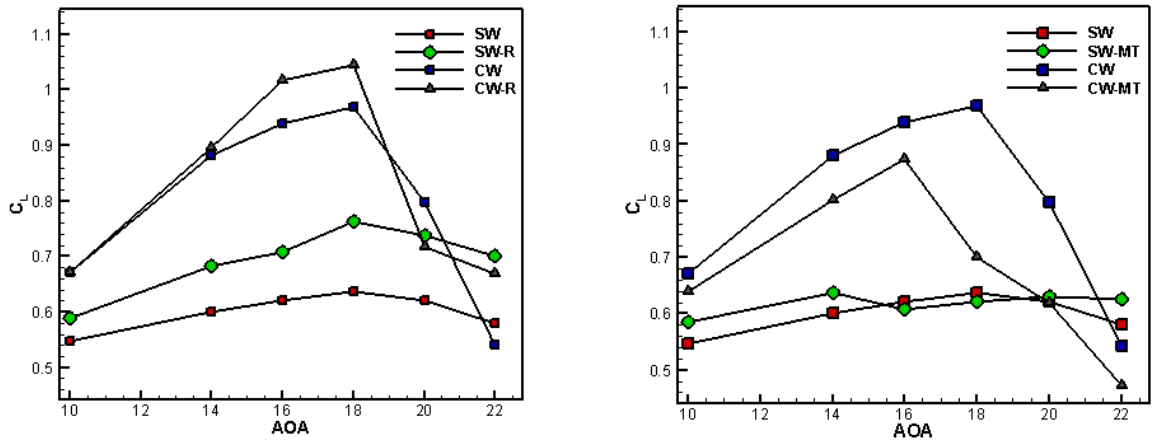

a b

Figure 8: Changes in the lift coefficient relative to the angle of attack for simple and sinusoidal wings a) Raked winglet b) Multi-tip winglet

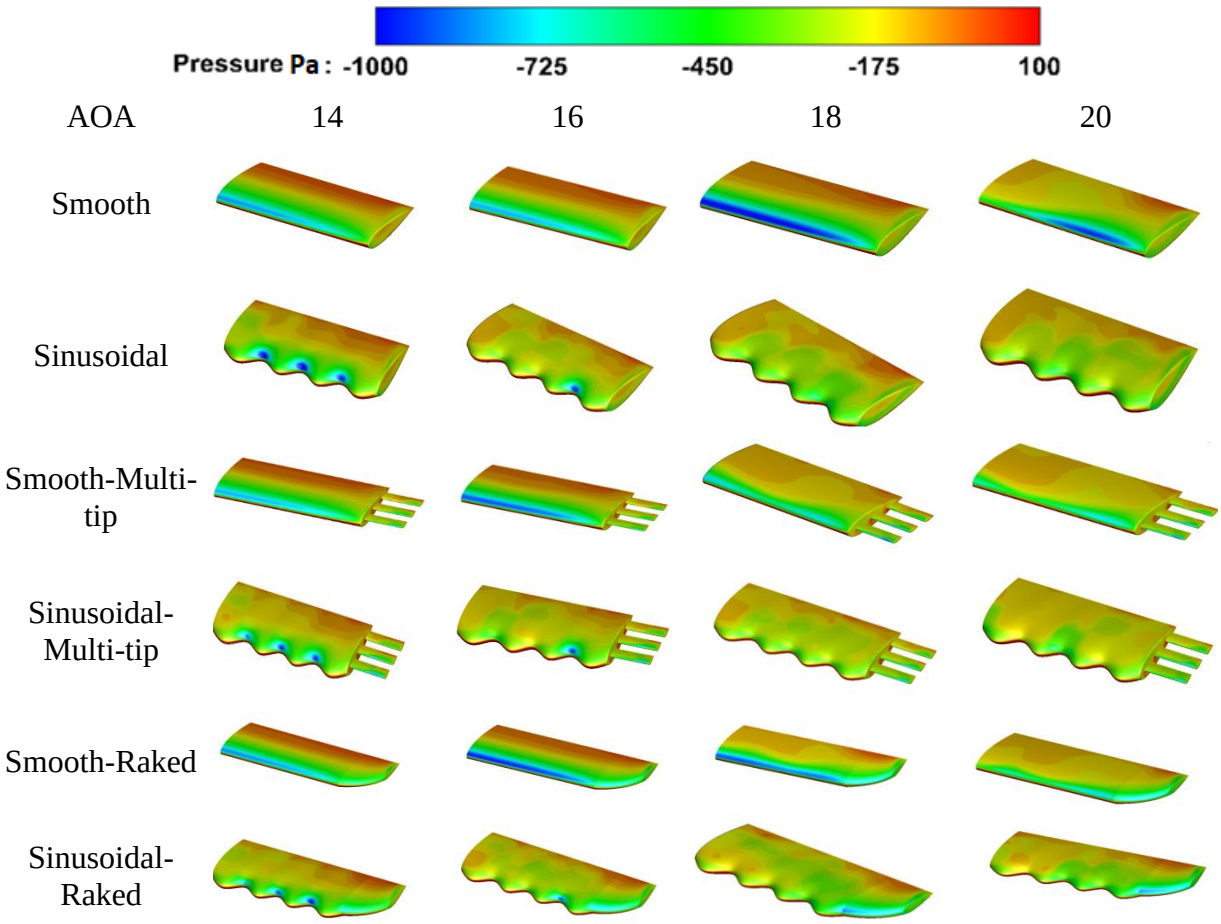

Figure 9: Distribution of pressure on the surface of different configurations

4.2. Parasitic Drag Coefficient

The effect of using winglets on the parasitic drag coefficient of simple and sinusoidal wings is investigated in Figure 10. This figure shows that the sinusoidal wing parasitic drag coefficient has increased compared to the simple wing in the stall range of 14 to 20 degrees. As can be seen in Figure 10-a, the parasitic drag coefficients of a wing with a sinusoidal edge without and with winglet from an angle of 14 to 20 degrees are greater than a simple wing, but at an angle of 22 degrees due to the complete separation of fluid flow on a simple wing, the parasitic drag coefficient of this wing is higher than the sinusoidal edge wing. Since increasing the aspect ratio for a wing with a winglet, parasitic drag increases under the same physical conditions (Figure 10-b). The parasitic drag force at 18 and 20 ° angles for the sinusoidal wing has a lower slope than the simple sinusoidal wing, which according to the contours of Figure 9 is due to low-pressure distribution changes in these two angles relative to each other.

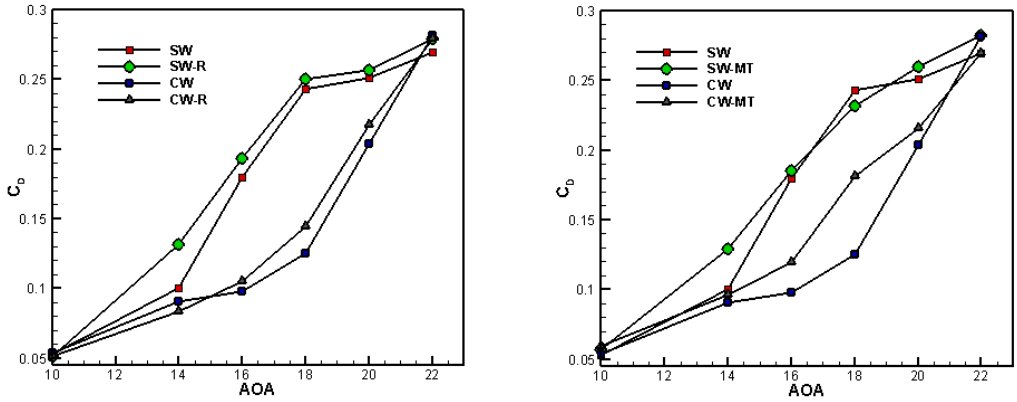

(a) (b)

Fig. 10: Changes in parasitic drag coefficient concerning the angle of attack around a simple and sinusoidal wing a) Raked winglet b) Multi-tip winglet

Due to the importance of mounting the winglet on the stall, Figure 11 shows the shear stress distribution on the surfaces of the various configurations to examine how the stall starts. According to the above figure, the use of winglets has affected the onset and spread of stalls. As can be seen, the use of a Multi-tip winglet further strengthens the separation in the middle region on the wing than the Raked winglet at the wings of the sinusoidal attack edge. Due to the collision of the flow with the peak and valleys , a rotational flow (inverse of each other) is induced, which creates two areas with different shear stresses.

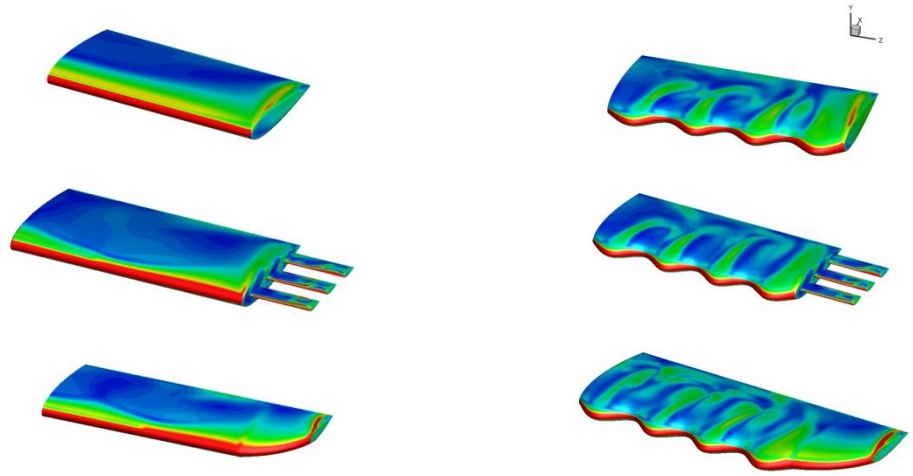

Figure 11: Shear stress distribution on the surface of different configurations at an angle of 18 degrees

According to the results of table 3, the use of a raked winglet for both wing configurations had a higher aerodynamic performance than multi-tip due to the increase in the $C_{L\max}$. But stall for multi-tip configurations occurred due to the reduction of the spanwise flow of faster flow at a lower angle than in the configuration without winglet.

Table 3: Performance of different configurations during stall

Wing	$(C_L / C_D)_{\max}$	$C_{L\max}$	α_{Stall}, deg	$\alpha_{C_{L\max}}$, deg
CW	7.73	0.9682	20	18
CW-R	7.95	1.045	20	18
CW-MT	7.3	0.8743	18	16
SW	3.08	0.6367	20	18
SW-R	3.56	0.7620	20	18
SW-MT	3.22	0.6374	16	14

4.3. Induced drag and vortices

In this section, a complete study of induced vortices around different configurations and comparing them with each other in terms of quality and quantitative analysis of the effect of possible changes on the induced drag coefficient is performed. For this purpose, first, the performance of the winglet on reducing the inductive vortices of the tip of each wing is investigated separately and then the distribution of vortices around the two main wings in the use of different winglets relative to each other is researched. To show the power and distribution of the vortices, six plates are created along the chord length as shown in Figure 12. The first plate is on the chord and the second plate is on

the trailing edge. The other four plates are produced with the same distance from each other (0.075 m) downstream.

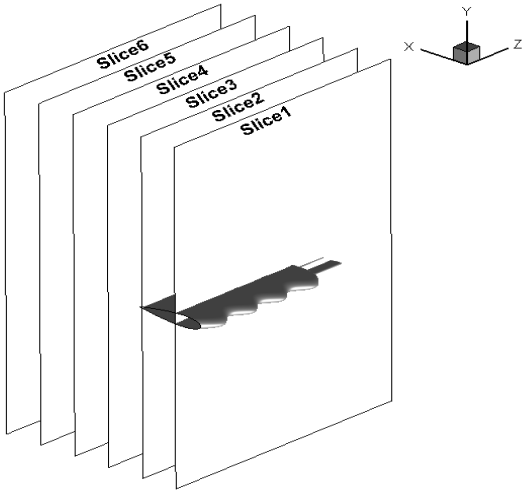

Figure 12: Geometric characteristics and names of sections produced around the wing

4.3.1. Effect of winglet on sinusoidal wing performance

According to the results of the sinusoidal wing with a Multi-tip winglet, the effect of this type of winglet on vortices has almost the same function as the simple wing. The behavior of the first vortex, resulting from the tip of the blades, for the sinusoidal edge wing has not changed and the curvature of the sinusoidal wing at the tip has increased the radius of the neutral vortex in the second vortex. The distinguishing feature of the Multi-tip winglet for the sinusoidal wing compared to the simple wing is the complete combination of the second vortex and the vortices resulting from the main wing surface at an angle of 22 degrees due to the lack of uniform distribution around the sinusoidal wing. According to Figure (14-b) before and after stall, the induced drag of sinusoidal edge wing with Raked winglet is more than simple sinusoidal edge wing and sinusoidal edge wing with Multi-tip winglet. As shown in Figure 13, similar to the simple wing, the use of a Raked winglet reduces the radius and strength of the central core of the vortices.

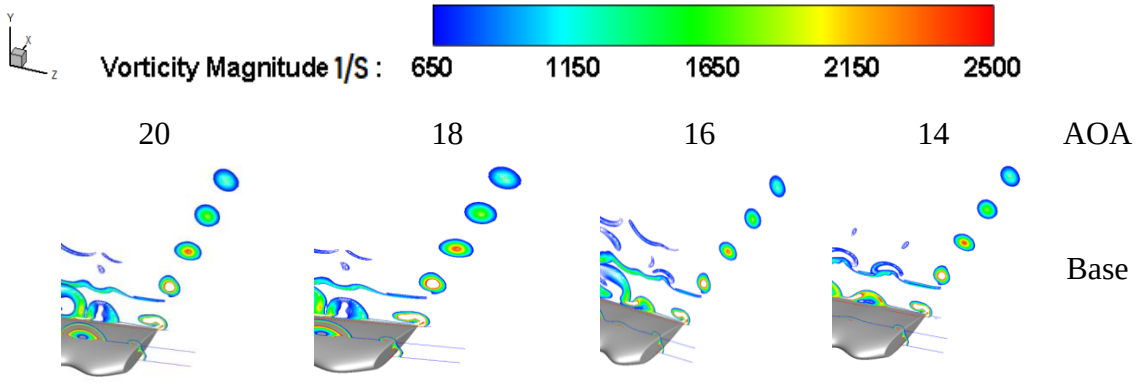

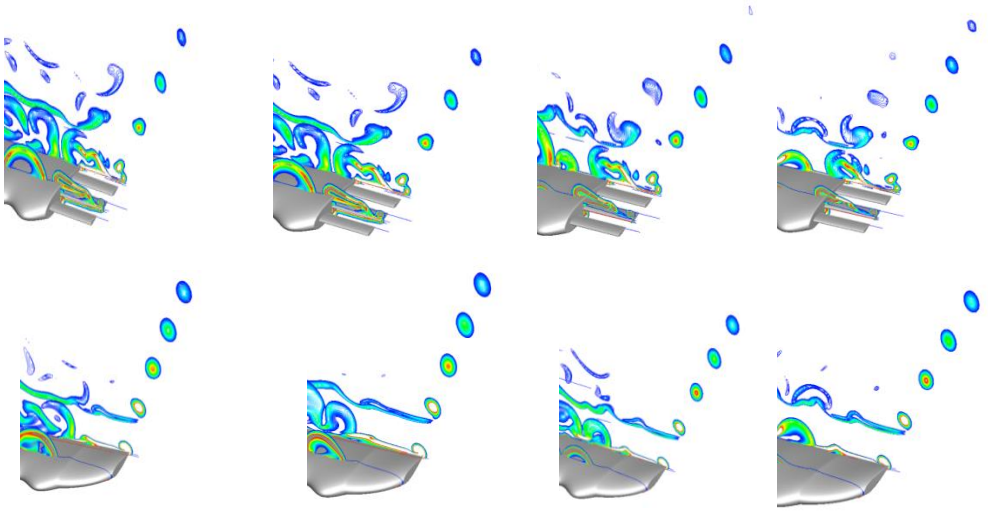

Figure 13: Effect of winglet use on inductive vortices of wing tip of sinusoidal attack edge

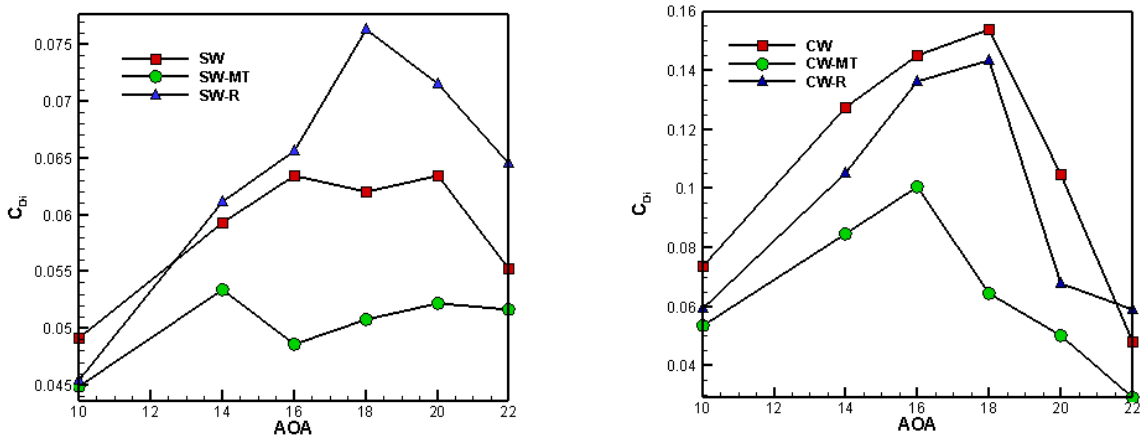

(a) (b)

Figure 14: Inducted drag coefficient changes a) Sinusoidal wing b) Simple wing

4.4.3. Analysis of the performance of simple and sinusoidal wings in the use of winglet

According to the presented results, the use of a winglet reduces the power and radius of the inductive vortex at different angles of attack around the simple wing. The same behavior is observed in the sinusoidal wing, and even the sinusoidal wing alone has been able to reduce the strength of vortices. This can be seen in section 1 of the shapes presented for winglets simple and sinusoidal wings for all the angles of attack studied. A noteworthy point has been the effect of winglets on the vortex distribution of the wings. The difference between the distribution of the vortex around the simple and sinusoidal wings at all angles of attack is due to the sinusoidal nature of the wings.

As can be seen in Figure 15, the change in flow arrangement when using a Multi-tip winglet for a sinusoidal wing relative to a simple wing intensifies the separation in the middle vortex of section 1, while due to the more uniform distribution of the vortex on the simple wing, the separation in

the cross-section 1 did not occur. By increasing the angle of attack to 18 degrees in Figure 16, more of the cross-section of the 1 sinusoidal wing with the Multi-tip winglet is affected by separation. The change in the fluid flow arrangement mentioned for the Multi-tip winglet is also less severe for the Raked winglet. At an angle of 18 degrees, the separation for both wings starts from the two parts of the root and the middle of the wing. With the onset of separation around the simple wing configurations and no return of fluid flow to the surface, it is observed that in sections 2 to 4 there are fewer vortices than in the sinusoidal wing configurations. With increasing angle of attack, the intensity of the mentioned changes increased to the point that at an angle of 22 degrees the vortices resulting from the Multi-tip winglet are combined with the vortices around both wing configurations in section 2. As shown in the section on aerodynamic coefficients, the induced drag decreases with decreasing lifting coefficient after stall and separation of fluid flow; in this section, it can be seen that induced vortices created at an angle of 22 degrees have less power than other angles.

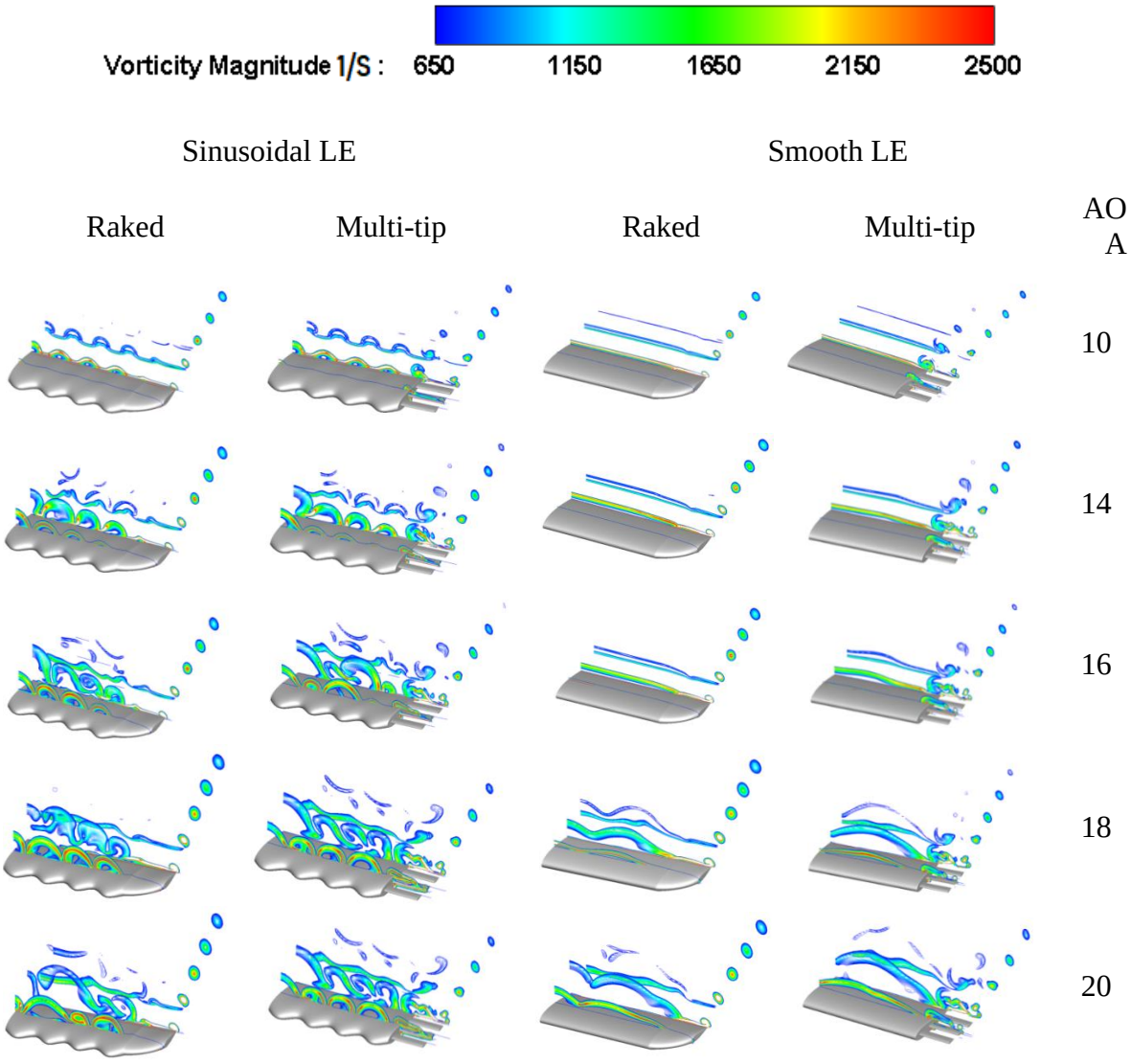

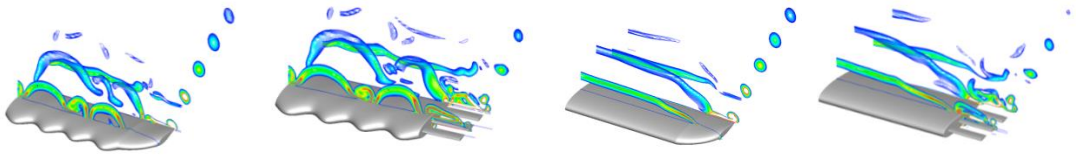

Figure 15: Vortices power distribution around different configurations

5. Investigation of induced Vortices behavior

Figures 16 and 17 show the behavior of induced vortices around a sinusoidal wing without winglet and with winglet at attack angles before and after stall. The $X/C=0$ and $X/C=0.5$ sections are produced in the middle of the chord and the trailing edge, respectively. The other surface is created at a certain distance from the trailing edge. On $X/C=0$, it can be seen that around the simple wing, wing without winglet, produced two vortices with different radius and attached to the wingtip. However, the curvature of the raked winglet before and after stall range prevents the formation of vortices, and the tips of a multi-tip winglet break the vortex into three vortices in the upper and lower regions of the winglet root and the tip of the tips radially far less than a simple wing. This difference between the radiuses of the vortices is exacerbated by the increasing angle of attack. When the flow reaches the $X/C=0.5$ two vortices around the simple wing are transformed into one another and a vortex is formed.

$X / C = 0$ $X / C = 0.5$ $X / C = 1$ $X / C = 1.5$

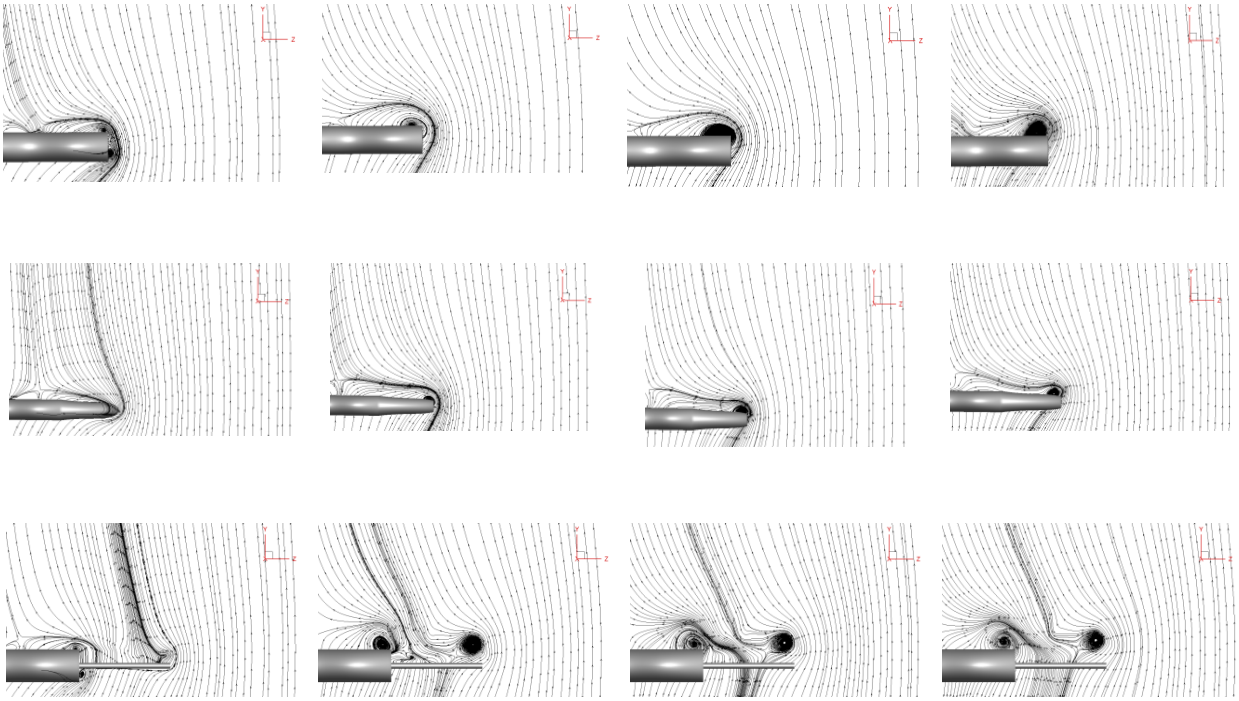

$X / C = 2$ $X / C = 2.5$

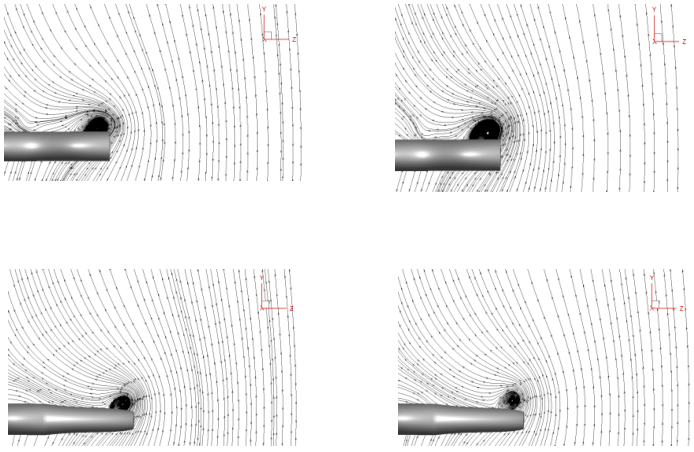

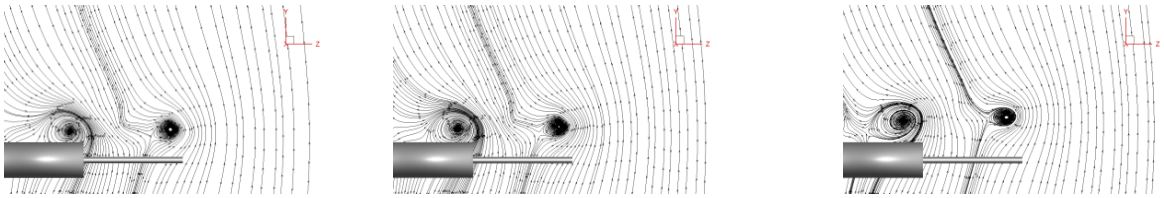

Figure 16: Investigation of the behavior of induced vortices at an angle of 14 degrees
Top:Without Winglet. mid:Raked. down:Multi-tip

This vortex has affected a smaller area before stall. But according to Figure 17, due to the separation of inductive vortex flow due to the difference in wingtip pressure with the induced vortex on the sinusoidal wing surface (Abrantes *et al*. 2017; Esmaeili *et al*. 2018; Bolzon *et al*. 2016), a larger area is affected by the vortices after stall. On the same plane, the radius of the vortices was less before the stall due to the further reduction of the secondary component flow around the raked winglet and after stall, due to further separation of the flow around the wing with a multi-tip, with the separation of the vortices from $X/C=1.5$ onwards the behavior of the multi-tip winglet has been better in reducing the radius of the vortices. This better behavior eliminates the vortices of the root and tip of the tips on pages $X/C=2$ and $X/C=2.5$. Accordingly, in Figure (15-a), the induced drag of the multi-tip winglet in the angles of attack of the stall range is reduced. In all configurations, the radius of the vortices has increased due to the addition of flow energy from the lower to the upper wing surface for $X/C=0.5$ and $X/C=1.5$. After that, the radius of the vortices has gradually decreased with the effect of fluid viscosity.

$X/C=0$ $X/C=0.5$ $X/C=1$ $X/C=1.5$

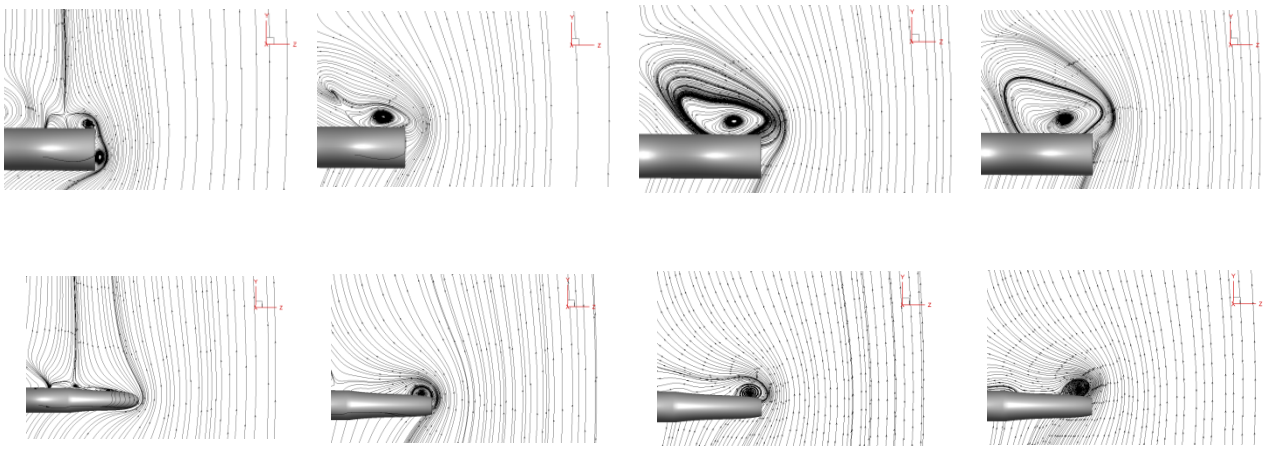

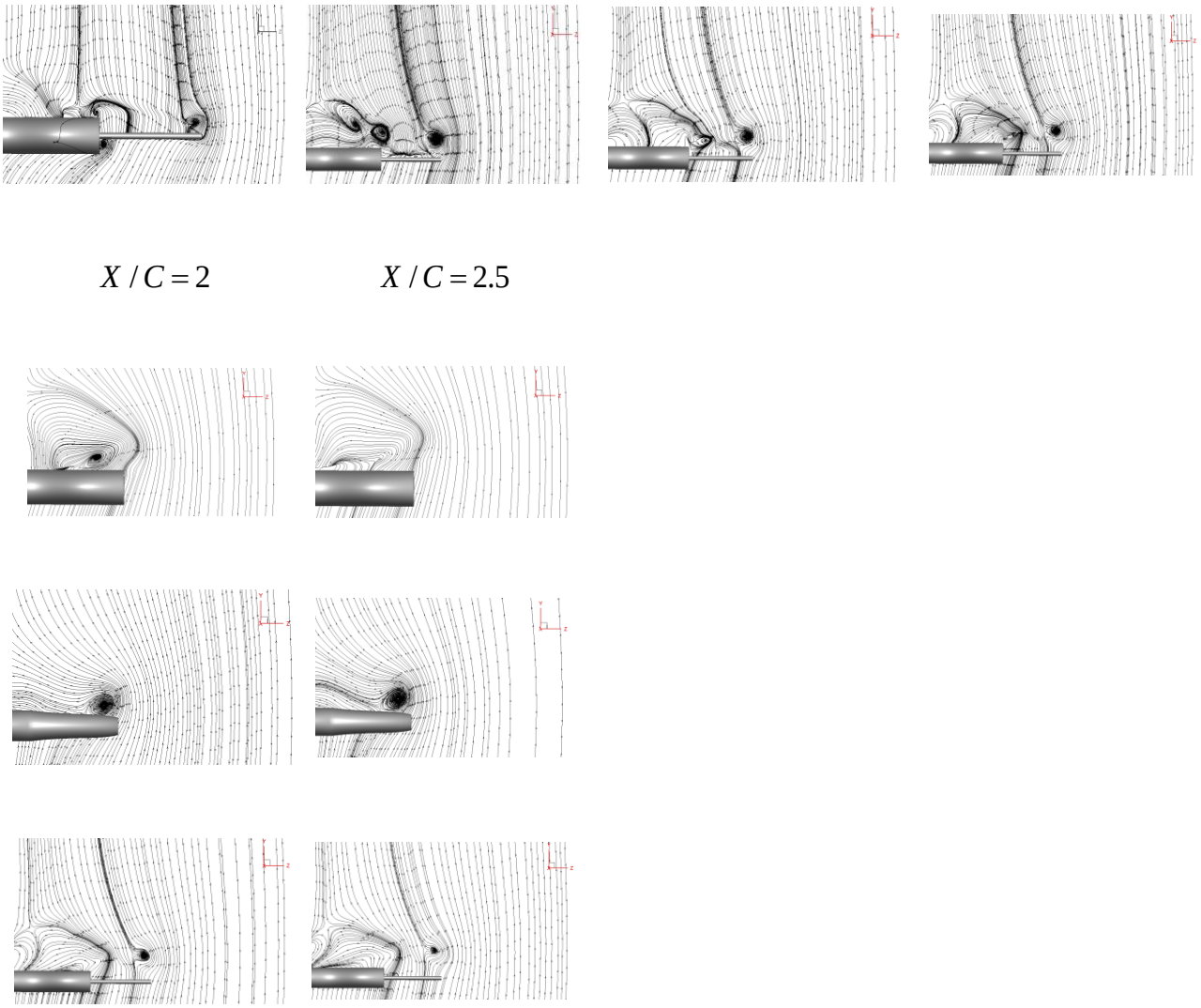

Figure 17: Investigation of the behavior of induced vortices at an angle of 22 degrees.
Top:Without Winglet. mid:Raked. down:Multi-tip

6. Conclusion

The main points of the results of this research are:

- The Raked winglet around both wing configurations produced more lifting force, and in contrast to the Multi-tip winglet, it had a less inductive drag.
- Installation of the winglet at the angles of attack examined for the simple wing and the wing with the sinusoidal attack edge has increased the drag force. However, the curvature of the attacking edge of the Raked winglet enhances the sinus wing function and reduces the slope of the drag coefficient changes after stall compared to the simple sinusoidal wing.
- Due to the lower lifting force of the Multi-tip winglet at all angles of attack, the aerodynamic performance of this winglet has been lower for both wing configurations examined during stall

and other angles of attack. However, Raked winglets increased aerodynamic performance by 5.12 and 2.28 percent on average in all studied attack angles around sinusoidal and simple wings.

- At an angle of 22 degrees, due to the complete separation of the fluid flow from the surface of the simple wing and the downward trend of the lift force coefficient with further increase of the angle of attack, the use of the winglet will not have a positive effect on aerodynamic performance. In contrast, due to the presence of part of the flow on the surface of the sinusoidal wing, the use of the winglet can affect the aerodynamic performance at this angle.
- The curvature of the sinusoidal wing at the attacking edge of the wing can reduce the power of inductive vortices relative to a wingless simple wing by choosing the correct amplitude and wavelength.
- The use of Multi-tip winglets around the sinusoidal wing at attack angles before stall has had a positive effect on reducing the strength and radius of the vortices, but with the onset of separation and afterward, the vortices around the sinusoidal wing gradually become stronger than the simple wing. While the Raked winglet, with its effect on the vortex root strength, had almost the same function in all angles of attack around both wings.

Reference

Abrantes, T. T. D. , Rios Cruz, A. A., de Paula, A. A., Kleine, V. G. and Büttner, F.,(2017) "The wing three-dimensional effects on wavy leading-edge performance," *in 35th AIAA applied aerodynamics conference*, p. 4467.

Aftab, S. M.A., Razak N.A., Mohd Rafie A.S. and Ahmad, K.A., (2016) "Mimicking the humpback whale: An aerodynamic perspective," *Progress in Aerospace Sciences*, vol. 84, pp. 48-69. 10.1016/j.paerosci.2016.03.002

Bolzon, M. D.P., Kelso R.M. and Arjomandi, M.(2016), " Formation of vortices on a tubercled wing, and their effects on drag," *Aerospace Science and Technology*, Vol. 56, pp. 46-55, https://doi.org/10.1016/j.ast.2016.06.025

Bravo-Mosquera, P. D., Cerón-Muñoz, H.D., Díaz-Vázquez, G. and Catalano, F.M., (2018) "Conceptual design and CFD analysis of a new prototype of agricultural aircraft," *Aerospace Science Technology*, Vol. 80, PP. 156-176. DOI: 10.1016/j.ast.2018.07.014

Carreira Pedro, H. and Kobayashi, M. (2008) "Numerical study of stall delay on humpback whale flippers," *in 46th AIAA aerospace sciences meeting and exhibit*, p. 584.

Chambers, J. R. (1990) "Concept to reality: contributions of the Langley Research Center to US Civil Aircraft of the US: NASA 2003, P. 306.

Dunning, J. B. Jr (2007), CRC handbook of avian body masses. CRC Press, 2007.

Esmaeili, A., Delgado, H. and Sousa, J. (2018), "Numerical simulations of low-Reynolds-number flow past finite wings with leading-edge protuberances," *Journal of Aircraft*, vol. 55, No. 1, PP. 226-238, DOI:10.2514/1.C034591

Gongzhang H. and Axtelius, E. (2020), "Aircraft Winglet Design Increasing the Aerodynamic efficiency of a wing", Kth Royal Institute of Technology School of Engineering Science.

Guerrero, J. E., Sanguineti, M., and Wittkowski, K. (2020), "Variable cant angle winglets for improvement of aircraft flight performance," *Meccanica*, vol. 55, no. 10, pp. 1917-1947, 2020. https://doi.org/10.1007/s11012-020-01230-1

Hassan, G., Hassan A. and and Elsayed Youssef M, (2014) "Numerical investigation of medium range re number aerodynamics characteristics for NACA0018 airfoil", CFD Letters, Vol. 6, No. 4, PP. 175-187

Horton, H. P.,(1968), "Laminar separation bubbles in two and three-dimensional incompressible flow," Queen Mary University of London. London E1 4NS

Hossain, A., Rahman, A. Hossen, J., Iqbal, A.K.M.P. , Zahirul, M.I., (2011) "Prediction of aerodynamic characteristics of an aircraft model with and without winglet using fuzzy logic technique," *Aerospace Science Technology*, Vol. 15, No. 8, PP. 595-605. https://doi.org/10.1016/j.ast.2010.12.003

Johari H, Henoch CW, Custodio D and Levshin A., (2007), "Effects of Leading-Edge Protuberances on Airfoil Performance". *AIAA Journal*, Vol.45, No.11, pp. 2634-2642. https://doi.org/10.2514/1.28497

Lynch, M. K. (2017), "Bio-Inspired Adaptive wing tip for low Reynolds number operation" Master of Science, Mechanical Engineering, University of Illinois at Urbana-Champaign, Urbana, Illinois.

Mehraban, A., Sayegh, Y. Djavareshkian, M.H., Fououzi Feshalami B. and Hassanalian, M. (2021), "Effects of smart flap on aerodynamic performance of sinusoidal leading-edge wings at low Reynolds numbers," *Proceedings of the Institution of Mechanical Engineers, Part G: Journal of Aerospace Engineering*, vol. 235, no. 4, pp. 439-450. https://doi.org/10.1177/0954410020946903

Merryisha S. and Rajendran, P. (2019), "Review of winglets on tip vortex, drag and airfoil geometry," *Journal of Advanced Research in Fluid Mechanics and Thermal Sciences*, Vol. 63, No. 2, pp. 218-237.

Miklosovic, D. Murray, M. Howle, L. and Fish, F., (2004), "Leading-edge tubercles delay stall on humpback whale (Megaptera novaeangliae) flippers," *Physics of Fluids*, Vol. 16, No. 5, pp. L39-L42, 2004. https://doi.org/10.1063/1.1688341

Munson, B. R., Okiishi, T. H., uebsch, W. W. H, and Rothmayer, A. P. (2016) " Fundamental Fluid Mechanics" Munson, 8 ed. USA: Wiley.Narayan, G. and Bibin, J. (2016) "Effect of winglets induced tip vortex structure on the performance of subsonic wings," *Aerospace Science Technology*, Vol. 58, PP. 328-340. https://doi.org/10.1016/j.ast.2016.08.031

New D. and Ng, B.F.(2020), "Flow control through bio-inspired leading-edge tubercles", Springer Nature Switzerland AG. Part of Springer Nature

Roy V. K. R. and Mukherjee A R, (2020), "Experimental validation of numerical decambering approach for flow past a rectangular wing," *Proceedings of the Institution of Mechanical Engineers, Part G: Journal of Aerospace Engineering*, vol. 234, no. 9, pp. 1564-1589, 2020.

Savile, D. J. E. (1957),"Adaptive evolution in the avian wing", pp. 212-224, 1957.

Sharafi, A., (2015), "Experimental Investigation of Grid Winglet Effects on Aerodynamic Characteristics of a Wing Model at Low Reynolds Number", *Journal of Aeronautical Engineering*, Vol 16, NO 2.

Versteeg H. K., Malalasekera, W.(2007), " An Introduction to Computational Fluid Dynamics, Second Edition ed. 2007. pearsoned.co.uk/versteeg

Whitcomb, R. T. (1976), "A design approach and selected wind tunnel results at high subsonic speeds for wing-tip mounted winglets," NASA, L-10908.

Wilcox, D. C., (1988), "Reassessment of the scale-determining equation for advanced turbulence models," *AIAA Journal*, Vol. 26, No. 11, pp. 1299-1310. https://doi.org/10.2514/3.10041

Yasuda, T., Fukui, K., Matsuo, K., Minagawa, H. and Kurimoto, R. (2019) "Effect of the Reynolds number on the performance of a NACA0012 wing with a leading-edge protuberance at low Reynolds numbers " *Flow, Turbulence and Combustion*, Vol. 102, No. 2, pp. 435-455.

Zhang, L., Dongli MA, Muqing Y., Shaoqi, W., (2020), "Optimization and analysis of winglet configuration for solar aircraft," *Chinese Journal of Aeronautics*, Volume 33, Issue 12, Pages 3238-3252. https://doi.org/10.1016/j.cja.2020.04.008

Zverkov, I.D., Zanin, B. Yu. and Kozlov, V. (2008), "Disturbances growth in boundary layers on classical and wavy surface wings," *AIAA Journal*, vol. 46, No. 12, pp. 3149-3158. DOI: 10.2514/1.37562